

Contents lists available at ScienceDirect

Advanced Powder Technology

journal homepage: www.elsevier.com/locate/apt



Original Research Paper

CFD simulations of natural convection particle-laden flow with CRW turbulent dispersion model employing the specialized solver containmentFOAM



Manohar Kampili^a, Stephan Kelm^a, Abdelouahab Dehbi^{b,*}, Xiongguo Liu^a, Hans-Josef Allelein^a

ARTICLE INFO

Article history: Received 10 May 2023 Received in revised form 4 March 2024 Accepted 28 May 2024 Available online 5 June 2024

Keywords: Turbulent dispersion Continuous random walk model Natural convection turbulent flows containmentFOAM

ABSTRACT

The Continuous Random Walk (CRW) model based on the normalized Langevin equation is often used to model the turbulent dispersion of particles wherein the flow field is computed using the RANS models. It has shown good accuracy in predicting overall particle deposition and the particle velocity statistics in forced convection turbulent flows. In the present paper, the CRW model is extended to predict particle transport in a natural convection flow (Ra 10^9). The validation is performed against the DIANA experiments performed at the Paul Scherrer Institute, Switzerland. The mean flow field is obtained systematically using the URANS approach (k- ω SST). The fluid near-wall turbulent statistics are obtained using correlations derived from the DNS data of Sebilleau et al. (2018). The results show that the CRW model is capable of predicting the particle deposition and distribution with reasonable accuracy for both 2.5 and 1 μ m particle sizes.

© 2024 The Society of Powder Technology Japan. Published by Elsevier B.V. and The Society of Powder Technology Japan. This is an open access article under the CC BY license (http://creativecommons.org/licenses/by/4.0/).

1. Introduction

Aerosol particle transport in turbulent flows is an important phenomena in many industrial as well as environmental applications. Though it is of considerable interest for indoor air quality in industries [1], commercial airline cabins [2], it has evolved as a topic of paramount importance in recent times of COVID-19 pandemic, especially in public places such as hospitals, airports and classrooms [3,4]. In addition to particle size and density determining the drag and gravity forces, the flow turbulence interaction in combination with the thermophoresis is a key mechanism governing the particles deposition and distribution in enclosures [5,6]. Indeed, particles are drawn to the walls by turbulence, and near the walls, temperature gradients are the highest, and hence thermophoresis in those regions will be significant and will tend to push particles towards or away from the walls depending on the sign of the gradients. Hence the combination of turbulence and thermophoresis is the dominant physical phenomenon which decides particles transport and fate in the case at hand. A similar relevance is also given to aerosol transport in nuclear reactor containment under typical severe accident conditions [7-10]. In

the put forth effort, the spotlight is on modeling the aerosol particles transport in turbulent natural convection flows under the assumption that the particles do not influence the flow field because of their very low concentration.

Particle transport in natural convection flows has been investigated over a long time experimentally and numerically. In the laminar flow regime, the particle transport is straightforward as the forces acting on the particles are deterministic. In case of turbulent flows, the particle transport is stochastic in nature due to the influence of turbulence. The impact of turbulent velocity fluctuations on the particle transport is dependent on the Stokes number (*Stk*), which is the ratio of particle relaxation time to flow turbulent time scale. A lower Stk indicates that the particles are able to follow the flow streamlines closely, whereas the higher Stk indicates that the particles deviate from the streamlines due to their inertia. Thus the variation of turbulent velocity fluctuations within the flow domain play a considerable role in determining the motion of particles. In the literature, Fevrier et al. (2005) [11] investigated particle-laden flows with the Stk ranging 0.02 to 10 interacting with isotropic turbulence, Goswami et al. (2011) [12] studied the dilute suspension flow with Stk ranging between 2.5 and 30 in forced convection turbulence using DNS calculations. In the similar range of Stk, Kulick et al. 1994 [13] performed experiments in fully developed channel particle-laden flow with Stk varying from 0.57

^a Institute for Energy and Climate Research (IEK-6), Forschungszentrum Juelich GmbH, 52425 Juelich, Germany

^b Laboratory for Scientific Computing and Modeling, Paul Scherrer Institut, 5232 Villigen, Switzerland

^{*} Corresponding author.

E-mail address: abdel.dehbi@psi.ch (A. Dehbi).

Nomenclature $\overline{U_f}$ Ra Rayleigh number (-) mean velocity of the fluid flow (m/s)gravitational acceleration (m/s^2) u_f^i fluctuating velocity of the fluid flow (m/s)g fluctuating velocity of the fluid flow in i^{th} direction thermal expansion coefficient (1/K) β_f и́і ŇΤ temperature difference between hot and cold walls (K)Lagrangian time scale in i^{th} direction (m/s)characteristic length of DIANA facility (m) I. τ_i kinematic viscosity of air (m^2/s) RMS velocity of the fluid flow in i^{th} direction (m/s)ν σ_i thermal diffusivity of air (m^2/s) dimensionless RMS velocity of the fluid flow in ith direcα σ_i^+ C(t)air-borne particle concentration at time t air-borne particle concentration at time 0 Lagrangian time scale (s) τ_{l} C_0 t time (s) τ_l^+ dimensionless Lagrangian time scale (-) τ particle deposition time constant (s) particle density (kg/m^3) particle deposition decay constant (1/s)thermal conductivity of fluid (W/m.K) V_{TS} particle terminal velocity (m/s) $\vec{k_p}$ thermal conductivity of particle (W/m.K)particle deposition decay constant from stirred settling К'n Kundsen number (-) β_{TS} Τ temperature of the fluid (K)model (1/s)particle deposition time constant from stirred settling Stk Stokes number (-) τ_{TS} u^+ dimensionless distance from the wall (-) model (s) particle relaxation time (s) dimensionless velocity parallel to the wall (-) τ_p m_p particle mass (kg) u_{τ} friction velocity (m/s)particle velocity (m/s) U_{p} x, y, zcartesian co-ordinates wall shear stress (N/m^2) drag force (N) F_D τ_w F_g F_T gravitational force (N) k turbulent kinetic energy (m^2/s^2) thermophoretic force (N)specific dissipation rate (1/s)ω C_C particle position vector T_h average hot wall temperature (K)Cunningham correction factor (-) average cold wall temperature (K) T_c drag coefficient (-) V_r circulation velocity of flow inside the DIANA cavity C_D particle diameter (m) D_p (m/s)fluid density (kg/m^3) dimensionless turbulence intensity (-) Ü_f fluid flow velocity (m/s)Lagrangian integration timestep (s) dt_{Lag} mean free path of air (m)particle Reynolds number (-) Re_p dynamic viscosity of air (Pa - s) μ_f

to 3.0. In the present work, the Stk of the particles are 1.21×10^{-5} and 6.94×10^{-5} for 1 μ m and 2.5 μ m diameters respectively. This represents the lower extreme of Stk spectrum. In case of enclosures with thermal gradients as in the present study, it is the combination of turbulent dispersion and thermophoresis which decides particle transport.

In the perspective of particle transport in enclosure flows (for both forced convection and natural convection), a notable review is given by Liu (2009) [14], which clearly shows that the particle transport in natural convection turbulent flow was only investigated sparsely. The majority of the experiments in this regard are performed with forced convection turbulence created by either a mixing fan or by continuous injection of fluid [14,15]. The experiments performed under the conditions of natural convection turbulence are found in Chen et al. (1992) [16], Thatcher et al. (1996) [17], Kalilainen et al. (2016) [15], and Kim et al. (2018) [2]. Due to the availability of experimental data in high resolution of space and time, the DIANA experiments of Kalilainen et al. (2016) [15] are chosen for the present CFD model development and validation. Additionally, these experiments are numerically investigated in using the Large Eddy Simulation (LES) approach by Dehbi et al. (2017) [18] which provide detailed insights needed for modeling. for instance the significance of wall-to-wall radiation heat transfer. It should be noted that the Kim et al. (2018) [2] experiments are an extension of the DIANA experiments and involve additional particle sizes and a different measurement method.

Fundamentally, there exists two approaches to model particle transport: the Euler-Euler approach and Euler-Lagrangian approach. While the former is typically used for dense particle

concentration flows, the latter is used for dilute particle-laden flows. In the present work, the Euler-Lagrange is employed due to the more intuitive specification and interpretation of boundary conditions as well as results. Within the Euler-Lagrangian approach, the Eulerian flow field can be obtained by one of the CFD techniques such as DNS, LES and URANS while the Lagrangian particles are tracked according to force balance in the obtained flow field. Using the DNS technique for computing the flow field and Lagrangian Particle Tracking (LPT), Pallares and Grau (2012) [19] showed that the interplay of gravity, and turbulent dispersion considerably impacts particle concentration and deposition in a turbulent natural convection channel flow. Along similar lines, Puragliesi et al. (2011) [20] used the DNS for computing flow field in differentially heated cavity and performed Lagrangian Particle Tracking (LPT) for various particle sizes to predict particle deposition. In the view of reducing the computational cost without losing significant accuracy, usage of LES technique for computing flow field has gained considerable importance recently. In the combination of LES for flow field and LPT for particle transport, Dehbi et al. (2017) [18], Kim et al. (2018) [2], Sayed et al. (2022) [21] used various LES models and validated them against the DIANA experimental data of Kalilainen et al. (2016) [15]. In both the experimental studies as well as the numerical studies, the key finding is that the turbulence influences particle deposition and distribution significantly depending on particle size. As the DNS and LES techniques employed resolve the flow field up to the influencing scales of particle motion, the models yield accurate results for particle transport without the need of turbulent dispersion models in the particle equations of motion.

In the view of large scale closed environments such as airports, conference halls and nuclear reactor containment, both the DNS and LES approaches are computationally expensive and maybe intractable. As a result, the URANS technique for the flow field is the preferred choice. However, the URANS technique cannot yield resolved turbulent structures which influence the particle motion especially in the wall boundary layer where turbulence is both anisotropic and inhomogeneous. In the literature, this problem is often overcome by appending a turbulent dispersion model on top of the mean flow field. A well-studied group of models in this regard are the Continuous Random Walk (CRW) models, which can be further classified into two groups: the first group of models is based on the dimensional Langevin equation and the second group of models based on the non-dimensional (normalized) Langevin equation. It is shown in many studies that the CRW model based on the normalized Langevin equation produced superior results in strongly inhomogeneous boundary layer turbulent flows. Hereafter the readers should note that the CRW model refers to the model based on the normalized Langevin equation. Dehbi (2008) [22] has studied the CRW model by including the drift correction term and applied it to simple pipe geometry as well as the complex mouth-throat geometry. The model has been further validated for turbulent pipe flows in the presence of strong thermophoresis in boundary layer by Dehbi (2009) [23]. Further, the model was validated for particle transport in channel flow in the work Dehbi (2010) [24] and in T-junctions by Dehbi (2011) [25] and in duct flows by Jayaraju et al. (2015) [26]. The model yielded good results also for a complex geometry of a steam generator rod bundle, as shown by Mukin et al. (2016) [27]. The model is further applied to compute the transport of particles as small as 10 nm in turbulent pipe flow by Mofakham et al. (2020) [28]. Recently improvements to the CRW model are proposed to extend the applicability to spatially developing flows by Lo et al. (2022) [29]. A common feature in all these studies is that the flow is driven by forced convection, and to the best of authors' knowledge, the CRW model has not been applied to natural convection flows in combination with URANS modeling. In strongly inhomogeneous flows such as in this case study, the normalized version of the Langevin equation is necessary, because the wide range of velocity scales in the boundary layer cannot be accurately captured with the dimensional Langevin equation. In the present work, this model is adapted (see Section 3.3) to compute turbulent dispersion in a natural convection turbulent flow of Rayleigh number 109. The model implementation, verification and validation are performed thoroughly in the view of developing a tailored CFD solver containmentFOAM (based on OpenFOAM-6) for reactor containment analyses [30], which was previously systematically validated for computing flow field including multi-species diffusion, radiation heat transfer, wall condensation in small and medium scale facilities [31-34]. It should be noted that the solver is rigorously verified against a number of simple test cases before its validation [30]. The algorithms and models within the containmentFOAM are tailored for the specific applications such as containment flows [35]. One of the objectives of present work is to extend the scope of containmentFOAM to enable analyzing particle transport in a typical containment flow.

Hereafter, the paper is structured as following: In the next section, essential details about the DIANA experiments such as experimental procedure, techniques and the measurement uncertainty are described. Thereafter, the CFD model is presented, with a brief description of Eulerian fluid flow and LPT modeling with emphasis on turbulent dispersion model in Section 3. In continuation, boundary and initial conditions, numerical methods and schemes, and mesh refinement analysis are illustrated in the same section. The systematic validation of fluid flow as well as the particle deposition are elucidated in Section 4. The results are further discussed

in comparison with the LES simulations of Dehbi et al. (2017) [18] in Section 5. At the end, the summary and conclusions are presented in Section 6.

2. DIANA experiment

The DIfferentially heated cavity with Aerosol in NAtural convection (DIANA) facility was a cubical enclosure with side length of 0.7 m, located at Paul Scherrer Institute, Switzerland [15]. The front view of DIANA facility is presented schematically in Fig. 1. The two vertical opposing walls were maintained at constant temperatures throughout the experiment. The flow inside the enclosure was driven by the buoyancy forces generated due to the temperature difference between the vertical walls, namely hot wall and cold wall. The hot and cold walls were made of aluminium and painted in black. In order to allow optical access, front and top walls consisted of two glass plates. The top and bottom walls were maintained close to convectively adiabatic boundary condition. The emissivity of the glass plates was 0.9 while the emissivity of vertical walls was estimated to be in the range 0.89-0.94. The flow field was measured by using Particle Image Velocimetry (PIV) with high resolution in space and time. The mean and RMS of velocity, and turbulence intensity were measured in the central x - y plane (z =0.35 m) of the DIANA facility and presented in Kalilainen et al. (2016) [15]. The temperature distribution in the fluid flow domain and in the walls were measured using K-type thermocouples. The average hot wall temperature (T_h) was estimated to be 330.6 K while the average cold wall temperature (T_c) was 291.3 K. The measured top and bottom walls temperature distribution is used as boundary condition for the current CFD simulation. The measurement uncertainty was 0.4 K. In addition to the wall temperatures, the gas temperatures were measured at five different heights (y = 0.07, 0.21, 0.35, 0.49 and 0.63 m) and along the central vertical line (x = 0.35 m). The temperature measurements locations is depicted in Fig. 2. Particle transport in DIANA facility was investigated by injecting silica (SiO $_2$) particles of size 1.0 μm and 2.5 μm and a density of 2000 kg/m³ separately. The particles concentra-

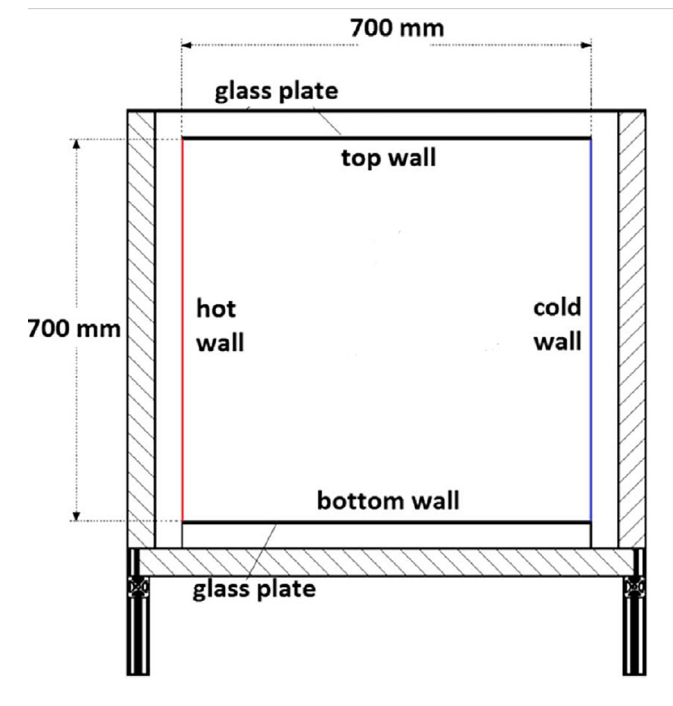


Fig. 1. Schematic of DIANA facility (front view) [15].

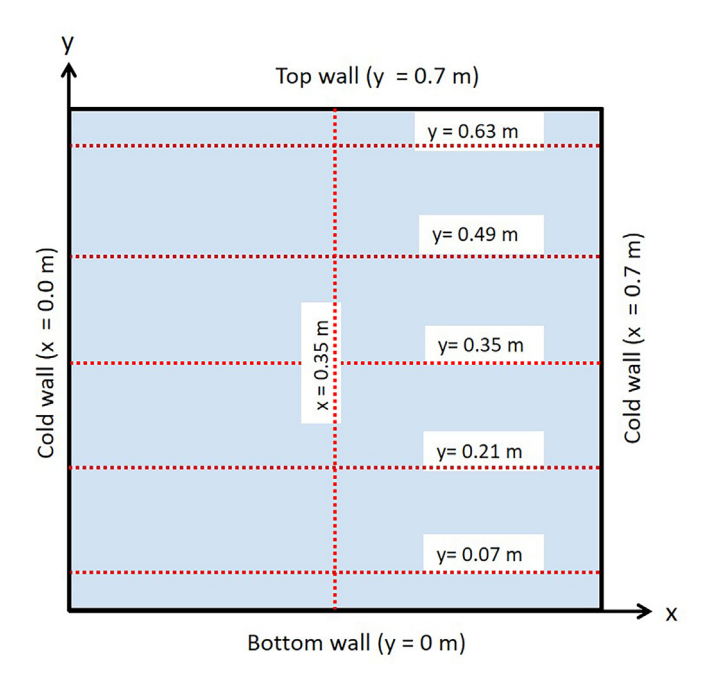


Fig. 2. Temperature measurements in DIANA facility.

tion variation with time was measured using two independent measurements methods: mass concentration and laser reflection by Kalilainen et al. (2016) [15]. The particle deposition rate was found to follow an exponential decay. These experiments were further repeated by Kim et al. (2018) [2] with an additional particle size of 0.5 μ m using intrusive ELPI technique (Electrical Low Pressure Impactor) and the results between the two investigations were consistent. In the present work, comparison is made between CFD simulations and experiments of Kalilainen et al. (2016) [15] and Kim et al. (2018) [2].

2.1. Flow and particle deposition characterization

Following the literature and the fundamentals of fluid mechanics, Kalilainen et al. (2016) [15] used the Rayleigh number (Ra) to characterize the buoyancy driven flow in DIANA experiments. The Rayleigh number is defined as the ratio of buoyancy forces to viscous forces as given in Eq. 1.

$$Ra = \frac{g\beta_f \Delta T L^3}{v\alpha} \tag{1}$$

where β_f is thermal expansion coefficient of the fluid, ΔT is the temperature difference between hot and cold walls, L is the side length of cubic enclosure, v is kinematic viscosity of the fluid, α is thermal diffusivity of the fluid. All the fluid properties are presented in Table 1 at a reference temperature, which is the average of hot and cold walls.

Le Qúeré and Behnia (1998) [36] performed DNS simulations of a two dimensional flow in a square cavity driven by the temperature differences between vertical walls and identified a critical *Ra* =

Table 1 Fluid properties at the reference temperature

Fluid property	Value
Thermal expansion coefficient (β_f)	$3.21 \times 10^{-3} \text{ K}^{-1}$
Kinematic viscosity (v)	$1.659\times10^{-5}m^2/s$
Thermal diffusion coefficient (α)	$2.36 \times 10^{-5} \ m^2/s$

 1.82×10^8 for transition into turbulent flow. The Rayleigh number is in the order of 10^9 for the buoyancy driven flow in the DIANA experiment, and hence it can be characterized as a natural convection turbulent flow.

In an enclosure flow, the particle deposition on various surfaces of the enclosure could be significant depending on the flow conditions. A measure of the amount of particle deposition on all the walls is obtained by computing the airborne particle concentration. According to Liu (2009) [14], airborne particle concentration in a enclosure follows an exponential decay as given by Eq. 2.

$$C(t) = C_0 \cdot e^{(-t/\tau)} \tag{2}$$

where C(t) is the airborne particle concentration at time t, C(0) is initial particle concentration in the enclosure, and τ is a time constant. The inverse of τ is called decay constant (β) and it represents the rate of deposition of particles on all walls of the enclosure. In the present work, decay constant (β) is derived from the simulations and compared with the experimental data of Kalilainen et al. (2016) [15] and Kim et al. (2018) [2].

3. CFD model

As the CFD model developed here is in the armature of a specialized solver of containment thermal-hydraulics, the baseline model, which is validated [31–33] in detail is utilized here. In this work, the limelight is on the extension of baseline model to particle-laden flows and systematic assessment on the accuracy of the overall model, besides thorough validation. The Eulerian-Lagrangian approach is chosen for its inherent benefits in interpreting the results and simplicity of boundary conditions related to particle transport.

3.1. Eulerian fluid flow

The complete CFD model, governing equations, default numerical settings associated with the containmentFOAM are described thoroughly in Kelm et al. (2021) [30] for single phase fluid flow. and hence only a brief description is outlined here. The modeling equations are established on unsteady Reynolds Averaged Navier Stokes (URANS) approach closed by the k-ω SST model. It should be noted that the production and dissipation terms corresponding to buoyancy force are included in the turbulence model in the view of application to technical scale facilities [32], equation derived based on the conservation of total enthalpy is solved for computing temperature field in the domain in conjunction with ideal gas equation. At first, the fluid flow inside the cavity is simulated until a time-averaged steady mean flow field conditions are established before injecting the Lagrangian particles. Thereafter, the Eulerian flow field and the LPT are solved one after another in each Eulerian integration time step.

The governing equations are solved with second order accurate spatial and temporal numerical schemes. As the open-source toolkit OpenFOAM comes with a large number of numerical schemes and methods, there is a possibility of user-induced error. Consequently, the numerical schemes are fixed and consistently used for many containment safety applications with the specialized CFD code *containmentFOAM*. For the discretization of transient terms, Crank-Nicolson scheme with a blending factor of 0.9 is used. The advection and gradient terms are discretized by applying Gauss linear upwind and Gauss linear schemes respectively. For the Laplacian (or diffusion) terms, Gauss linear scheme is employed with non-orthogonal correction.

The readers are referred to Kelm et al. (2021) [30], Kampili et al. (2021) [32] and Vijaya Kumar et al. (2020) [31] for detailed description on the numerical methods, solvers and algorithm,

which are well validated and used for the Eulerian fluid flow in the present work.

3.2. Lagrangian Particle Tracking

Initially, the particles are assumed to be uniformly distributed inside the cavity. All the particles are considered as spherical point masses. The particle velocities are computed in a flow field, which is constant within an Eulerian integration time step, by time integration of the Newton's second law of force balance (Eq. 3) with a Lagrangian integration time-step in the order of particle relaxation time (τ_p) for numerical accuracy. Thereafter, particle positions are updated according to the definition of velocity (Eq. 4). Within the present work, the Lagrangian integration time step is at least one order smaller than the Eulerian integration time step. Consequently, there are a number of Lagrangian integration cycles within one Eulerian integration time step.

$$m_p \frac{dU_p}{dt} = F_D + F_g + F_T \tag{3}$$

$$\frac{dx_p}{dt} = U_p \tag{4}$$

 x_p is particle position, m_p is particle mass, U_p is particle velocity, F_D is drag force, F_g is gravitational force (and buoyancy force), and F_T is thermophoretic force. After tracking the particles until the Eulerian integration time step is reached, the flow field is updated by solving the URANS equations using the PISO algorithm. Thereafter, the LPT is continued again to reach the next Eulerian intregation time step and so on. In the frame work of modeling nuclear aerosol transport (particle size: 0.2 μm to 10 μm), drag, gravity, and thermophoretic forces are considered as the dominant influencing forces. Brownian motion, pressure gradient, virtual or added mass forces have only minor impact in gas-solid particle-laden flows [18,2]. The lift force is not considered in modeling as it was proven to be negligible for particles in diffusion-impaction regime by Bagheri et al. (2012) [37] in a similar setup to DIANA, which is strengthened further by Dehbi et al. (2017) [18], Kim et al. (2018) [2], Aksouh et al. (2018) [7]. The drag force (F_D) is modeled according to Schiller and Naumann (1933) [38] as:

$$F_D = C_C C_D \frac{\pi D_p^2}{8} \rho_f (U_f - U_p) |U_f - U_p|$$
 (5)

where C_C is Cunningham correction factor, C_D is drag coefficient, D_p is diameter of the particle, ρ_f is fluid density, and U_f is fluid velocity. The C_C considerably changes the drag force for sub-micron particles and the standard expression for C_C is given as

$$C_C = 1 + \frac{2\lambda}{D_p} \left(1.257 + 0.4 \exp\left(\frac{-0.55D_p}{\lambda}\right) \right)$$
 (6)

where λ is mean free path of the fluid. An important parameter in calculating the drag force is drag coefficient (C_D) defined as a function of particle Reynolds number (Re_p) as following:

$$C_{D} = \begin{cases} \frac{24}{Re_{p}} \left(1 + 0.15Re_{p}^{0.687} \right), & \text{if } Re_{p} \leqslant 1\\ 0.44, & \text{if } Re_{p} > 1 \end{cases}$$

$$Re_p = \frac{\rho_p |U_f - U_p| D_p}{\mu_f} \tag{7}$$

where ρ_p is particle material density and μ_f is fluid dynamic viscosity. It must be noted that U_f is fluid velocity interpolated to the particle position from the grid points near to the particle current location in the numerical mesh. In case of a turbulent flow, it can be split into two parts: mean velocity $(\overline{U_f})$ and fluctuating velocity

 (u'_f) . The $\overline{U_f}$ is the mean velocity predicted from the URANS CFD simulation. The u'_f is the turbulent fluctuation velocity which is modeled using a turbulent dispersion model discussed in the following subsection.

The standard implementation of gravitational force along with the buoyancy force acting on a spherical particle in OpenFOAM-6 is as following [39]:

$$F_g = \frac{\left(\rho_p - \rho_f\right)\pi D_p^3 g}{6} \tag{8}$$

where g denotes the gravitational acceleration. The state of the art expression for the thermophoretic force (F_T) is taken from Talbot et al. (1980) [40] as given in the Eq. 9.

$$F_{T} = -\frac{6\pi\mu_{f}^{2}D_{p}C_{s}\left(\frac{k_{f}}{k_{p}} + C_{t}Kn\right)}{\rho_{f}(1 + 3C_{m}Kn)\left(1 + 2\frac{k_{f}}{k_{p}} + 2C_{t}Kn\right)}\frac{\nabla T}{T}$$
(9)

where T is temperature of the fluid, k_f is thermal conductivity of fluid, k_p is thermal conductivity of particle, Kn is particle Knudsen number, and C_s , C_t and C_m are modeling coefficients, set as 1.17, 2.18 and 1.14 respectively. The Knudsen number is defined as the ratio of mean free path of the fluid (λ) to diameter of the particle (D_p) as following:

$$Kn = \frac{\lambda}{D_p} \tag{10}$$

In the present simulations, the fluid under consideration is air and mean free path (λ = 0.69 nm) is considered as constant there is no significant variation in the pressure and temperature from the atmospheric conditions.

3.3. Turbulent dispersion model

The Langevin equation is originally proposed by Paul Langevin to model Brownian motion of very small particles. In its essence, the equation describes random motion of a Lagrangian particle in fluid due to collisions with fluid molecules. Obukhov (1959) [41] extended this concept to model fluid velocity fields in homogeneous turbulence using Markov chains. The conventional form of the Langevin equation is as following:

$$du_i = -\frac{u_i}{\tau}dt + d\mu_i \tag{11}$$

where u_i is fluid velocity fluctuation, τ is Lagrangian time scale and $d\mu_i$ is a random fluctuation, which requires suitable formulation depending on the application. As shown by Thompson et al. (1971) [42], the Langevin equation model is capable of accurately computing velocity fluctuation in homogeneous turbulence field. This approach is further extended in Wilson et al. (1981) [43], Legg and Raupach (1982) [44], Thomson (1984) [45] etc. to compute velocity fluctuations in inhomogeneous turbulence, by normalizing the Langevin equation. The underlined approach in the formulations of fluctuation term is replacing the term $d\mu_i$ term with its moments. According to Iliopoulos et al. (2003) [46], the normalized Langevin equation can be written as following:

$$d\left(\frac{u_i}{\sigma_i}\right) = -\left(\frac{u_i}{\sigma_i}\right)\frac{dt}{\tau_i} + d\eta_i + A_i dt \tag{12}$$

where σ_i is the RMS of velocity, $A_i dt$ is the first moment of the fluctuation term, and $d\eta_i$ is second moment. The subscript i denotes the direction in general, and the subscripts 1,2 and 3 are used to represent streamwise, wall-normal and spanwise directions separately in the boundary layer flow. Other higher order moments are neglected. Consequently, A_i can be written as following:

$$A_{i} = \frac{\left(\frac{\overline{u_{2}u_{i}}}{\sigma_{i}}\right)}{\partial x_{2}} \tag{13}$$

while the $d\eta_i$ term which is derived assuming joint Gaussian distribution up to first order (Mito and Hanratty 2002 [47]), can be expressed as following:

$$\overline{d\eta_i d\eta_i} = \frac{\overline{u_i u_j}}{\sigma_i \sigma_i} \left[\frac{1}{\tau_i} + \frac{1}{\tau_i} \right] \cdot dt \tag{14}$$

The A_i term is the mean drift correction and in the wall-normal direction it can be simplified to $\partial \sigma_2/\partial x_2$. It is shown in Thomson (1987) [48] and Mito and Hanratty (2002) [47] that the inclusion of this term fulfills the well-mixed criterion, i.e. that tracer particles which are well-mixed initially in the inhomogeneous turbulent flow, remain well-mixed. Further modeling improvements are made to track inertial particles by introducing a multiplicative factor, which is a function of Stokes number (Stk). A3 is set to zero according to Mito and Hanratty (2004) [49]. Only a short description is given here to enable to reader with basic understanding of Langevin equation inspite of profuse amount of research in the literature over the past decades. For complete details related to mathematical model development, simplifications and derivations, readers are referred to Dehbi (2008) [22]. Following the simplifications on normalized Langevin equation, the governing equations for computing velocity fluctuations seen by a particle are formulated into two sets depending on the particle position in flow. The governing equations to model fluid velocity fluctuations seen by the particles are described next. These fluctuations are combined with the mean flow velocities in the particle equations of motion to deduce particle trajectories, there after, the governing equations for particles located in the core flow are described. Governing equations in the boundary layer

$$d\left(\frac{u_1}{\sigma_1}\right) = -\left(\frac{u_1}{\sigma_1}\right) \cdot \frac{dt}{\tau_1} + \sqrt{\frac{2}{\tau_1}} \cdot d\zeta_1 + \frac{\partial\left(\frac{u_1u_2}{\sigma_1}\right)}{\partial x_2} \cdot \frac{dt}{1 + Stk}$$
 (15)

$$d\left(\frac{u_2}{\sigma_2}\right) = -\left(\frac{u_2}{\sigma_2}\right) \cdot \frac{dt}{\tau_2} + \sqrt{\frac{2}{\tau_2}} \cdot d\zeta_2 + \frac{\partial \sigma_2}{\partial x_2} \cdot \frac{dt}{1 + Stk}$$
 (16)

$$d\left(\frac{u_3}{\sigma_3}\right) = -\left(\frac{u_3}{\sigma_3}\right) \cdot \frac{dt}{\tau_3} + \sqrt{\frac{2}{\tau_3}} \cdot d\zeta_3 \tag{17}$$

$$Stk = \frac{\tau_p}{\tau_L} \tag{18}$$

where u_1,u_2,u_3 are components of the turbulent velocity fluctuation. The key parameters in the model are RMS velocity profiles $(\sigma_1,\sigma_2 \text{ and } \sigma_3)$ and Lagrangian time scales $(\tau_1,\tau_2 \text{ and } \tau_3)$, whose spatial variation allows to account for anisotropic and inhomogeneous turbulence. Similar to Dreeben and Pope correlations for forced convection turbulent flows, the RMS velocity profiles are obtained by curve fitting to the DNS data as functions of non-dimensional wall distance (x_2^+) . The friction velocity (u_τ) is used as a reference for non-dimensionalizing the RMS velocity components. The x_2^+ and u_τ are defined as in Eqs. 19 and 20.

$$x_2^+ = \frac{y \cdot u_\tau}{\nu} \tag{19}$$

$$u_{\tau} = \sqrt{\frac{\tau_w}{\rho}} \tag{20}$$

It is important to accurately input the RMS values for turbulent fluctuations in streamwise, wall-normal and spanwise directions based on DNS (or) LES (or) experimental data suitable for the geometry.

For forced convection turbulent pipe flows, the turbulent fluctuation RMS values and time scales do not vary significantly with Revnolds number (Re) of the flow. In this perspective, Dreeben and Pope correlations can be used as generic profiles for turbulent forced convection pipe flows [23]. However, for natural convection turbulent flows such generic correlations are not available for two reasons. One is the significant variation of turbulent fluctuations with Ra. The second one is variation of turbulent fluctuations along the vertical walls and the resulting difficulty in scaling. In the present work, only one Ra=10⁹ number flow field and the corresponding DNS data is used in deriving the RMS velocity correlations. The second issue is overcome by using averaged RMS velocity profiles from the DNS data at various heights. The correlations are derived using least squares method for curve-fitting as ratios of third and fifth order polynomials based the DNS data of Sebilleau et al. (2018) [50]. The RMS velocity profiles at various heights and their averaged curve fits are plotted together in Fig. 3. The left and right panels in this figure depict the RMS velocity profiles in the hot wall and cold wall boundary layers respectively. It should be noted that the RMS profiles variation along the hot wall height is higher than that of the cold wall. However, the averaged velocity profiles are nearly identical. As a consequence, the averaged correlations are suitable for both the hot and cold walls. The velocity fluctuations along the adiabatic horizontal wall are not considered in the present model as there is only a minor deposition on the top wall. On the bottom wall, the major deposition is due to the gravitational force. Within the scope of present work, it is assumed that the turbulent dispersion influence on particle deposition along the horizontal walls is negligible.

The curve fits are developed based on the turbulence statistics within the boundary layer. In Fig. 3, x_2^+ is non-dimensional wall distance, σ_1^+ is non-dimensional RMS velocity fluctuation in the vertical direction (parallel to the hot and cold walls), σ_2^+ is non-dimensional RMS velocity fluctuation in the wall-normal direction to the hot and cold walls. The $\overline{u_1u_2}^+$ is non-dimensional cross product term from RMS velocities in the wall-parallel (vertical) and wall-normal velocities, needed for the third term in Eq. 15. In the present work, the turbulent fluctuations in the lateral direction (u_3) are not considered as the fluid motion in this direction is negligible, i.e, flow is mostly two-dimensional. Consequently, the particle motion is mostly expected to be two-dimensional.

It is possible to estimate the Lagrangian time scales variation by tracking of fluid particles in DNS flow field [22]. For forced convection flows, Bocksell and Loth (2006) [51] used this method and concluded that Lagrangian time scales are comparable in all the directions ($\tau_1 = \tau_2 = \tau_3 = \tau_l$) and they are reasonably close to the correlations provided by Kallio and Reeks (1989) [52] in the non-dimensional form. However, such Lagrangian simulations in the natural convection DNS flow field are not performed/available in the literature to date. In the present work, the Lagrangian time scales correlations provided by Kallio and Reeks (1989) [52] shown in Eqs. 21 and 22 for forced convection turbulent flows, are utilized also for the natural convection turbulent flows. Consequently, there exists a possibility to improve the model further provided more accurate correlations for Lagrangian time scales variation are available.

$$\tau_l^+ = 10, \quad x_2^+ \leqslant 5$$
 (21)

$$\tau_1^+ = 7.122 + 0.5731x_2^+ - 0.00129y^{+2}, \quad 5 \leqslant x_2^+ \leqslant 100$$
 (22)

where τ_l^+ is non-dimensional Lagrangian time scale, defined as following:

$$\tau_l = \tau_l^+ \frac{v}{\left(u_\tau\right)^2} \tag{23}$$

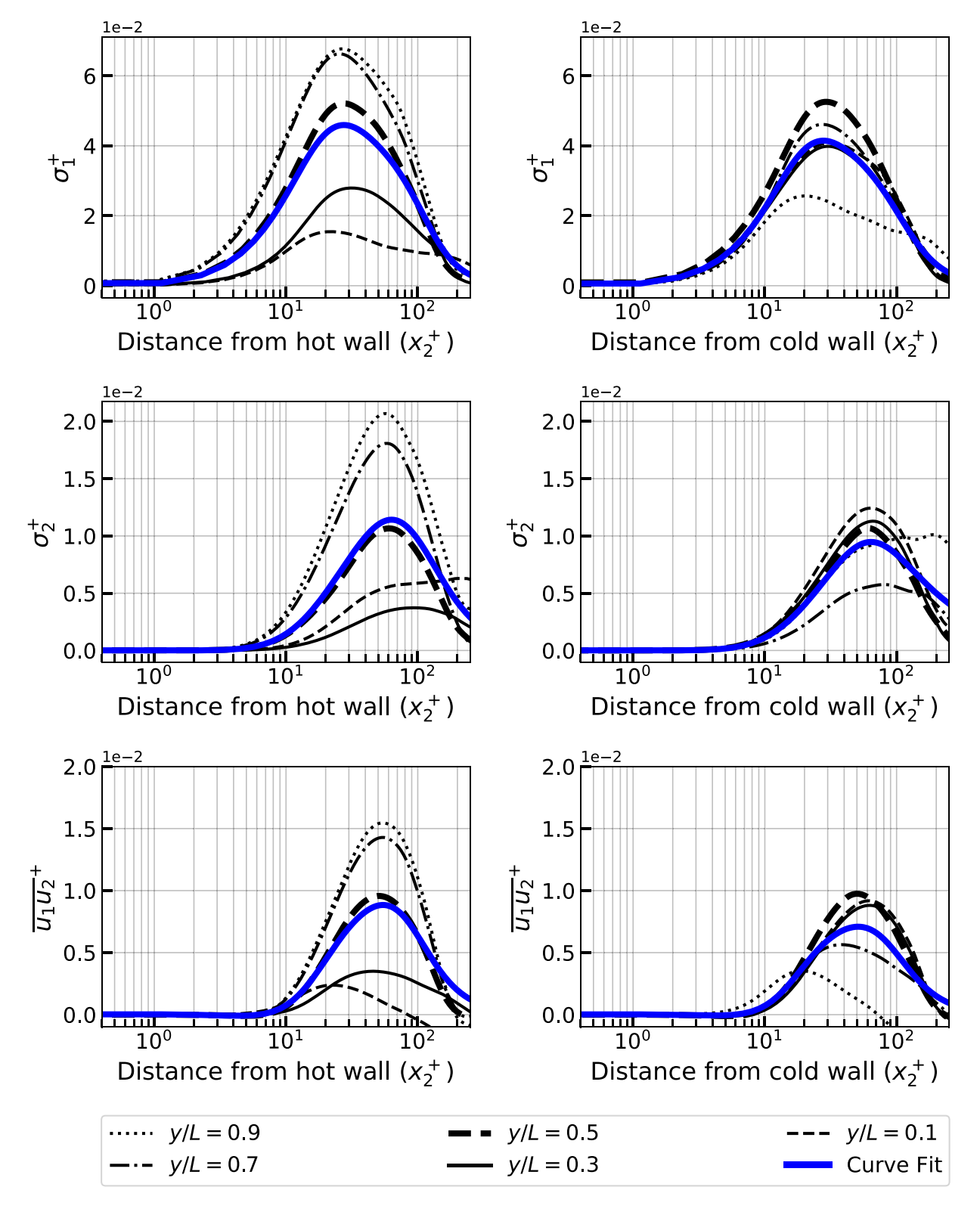


Fig. 3. Curve fits to the DNS data of Sebilleau et al. (2018).

Governing equations in the bulk flow

In the bulk turbulent flow, the CRW model utilizes the assumption of isotropic turbulent fluctuations. The RMS of velocity fluctuation is computed as a function of the turbulent kinetic energy (k) as $\sigma = \sqrt{\left(u_f'\right)^2} = \sqrt{\frac{2k}{3}}$. The governing equations for computing the

turbulent fluctuation velocity seen by a particle under isotropic turbulence assumption are given in Eq. 24.

$$d\left(\frac{u_i}{\sigma}\right) = -\left(\frac{u_i}{\sigma}\right) \cdot \frac{dt}{\tau_L} + \sqrt{\frac{2}{\tau_L}} \cdot d\zeta_i + \frac{1}{3\sigma} \cdot \frac{\partial k}{\partial x_i} \cdot \frac{dt}{1 + Stk}$$
 (24)

The turbulent kinetic energy (k) predicted by the URANS model is used as a collective measure of turbulent fluctuations in all the directions. The time scales of the flow are evaluated on the basis of turbulent kinetic energy k and turbulence dissipation rate ϵ according to Mito and Hanratty (2002) [47]. As the present work utilizes k- ω SST model, it is formulated in terms of ω as following:

$$\tau_L = \frac{2}{C_o} \cdot \frac{k}{\epsilon} = \frac{2}{C_o} \cdot \frac{1}{C_u \omega}$$
 (25)

The C_o value is approximated as 14 based on the DNS of forced convection turbulent flow simulations data by Mito and Hanratty (2002) [47] and the C_μ standard value is 0.09. With regards to present work, the turbulence in the inner core of the differentially heated cavity is very low in comparison to the turbulence in the boundary layer. Additionally, the k- ω SST models under-predicts the turbulence levels. In this perspective, the turbulent dispersion model in the inner core of the flow is insignificant for overall particle deposition as well as the distribution. The model governing equations are presented here for the sake of completeness and with the view of applicability to complex geometries where the turbulence in the inner core (locally) is relatively high and predictable from the URANS simulations.

The governing equations for LPT (Eqs. (3), (4), (15)–(17) and (24)) are numerically integrated using first order Euler implicit method with a constraint on the Lagrangian integration time step as minimum of one third of particle relaxation time or 10^{-6} s to ensure the accuracy of LPT. The constraint on time step as well as the numerical method are chosen based on the turbulent dispersion model development and validation by Dehbi (2008) [22], Dehbi (2009) [23], Dehbi (2010) [24] and Kampili et al. (2019) [53]. A second order linear interpolation scheme is employed to compute the fluid flow variables at the position of particles.

3.4. Initial and Boundary conditions

The cubical domain of DIANA facility is considered for numerical simulation without any scaling. The initial and boundary conditions used in the simulation are depicted in Fig. 4.

The initial conditions of the air inside the cavity are zero velocity in the domain and atmospheric pressure. The boundary conditions regarding the pressure and velocity at all the walls are atmospheric pressure and no slip velocity. For the left and right vertical walls shown in the Fig. 4, constant temperature boundary condition is used with the values of 330.6 K and 291.3 K respectively. For the top and bottom walls in DIANA facility, temperature profiles obtained from the experimental data (shown in right panel of Fig. 4) are given as boundary conditions. For the remaining walls of the cavity, convectively adiabatic boundary conditions are maintained. The wall to wall radiation heat transfer is considered by defining the measured temperature distribution on top and bottom walls from the experiment. This method of considering the radiation heat transfer is validated using LES simulations by Kim et al. (2018) [2]. One should note that the impact of radiation heat transfer is found to be significant even in the moderate temperature differences as in the present DIANA facility [2.54]. The particles are assumed to be sticking to the walls when they strike the walls.

3.5. Numerical grid and Grid convergence study

The grid convergence study is performed to assess the numerical error associated with the simulations. The fluid flow calculations are performed with three different meshes namely coarse, medium and fine meshes with second order spatial and temporal discretization schemes. Each mesh consists of structured hexahedral (cuboid) blocks. The mesh refinement is performed by dividing each cell into two halves in each direction, leading to a eight fold increase in the total number of cells from coarse mesh to medium mesh. The same is true for the medium mesh to fine mesh refinement. The meshes are created following the best practice guidelines for the application of CFD simulations in nuclear reactor safety by Mahaffy et al. (2014) [55]. Summary of the mesh quality assessment parameters is provided in Table 2. From the initial conditions, the flow field is allowed to reach statistically stationary conditions by simulating up to 600 non-dimensional time units, similar to previous LES simulations of Dehbi et al. (2017) [18]. A non-dimensional time unit (τ) is defined as the ratio of side length of cube (L) to the circulation velocity of flow (V_r) as in Eq. 26. The

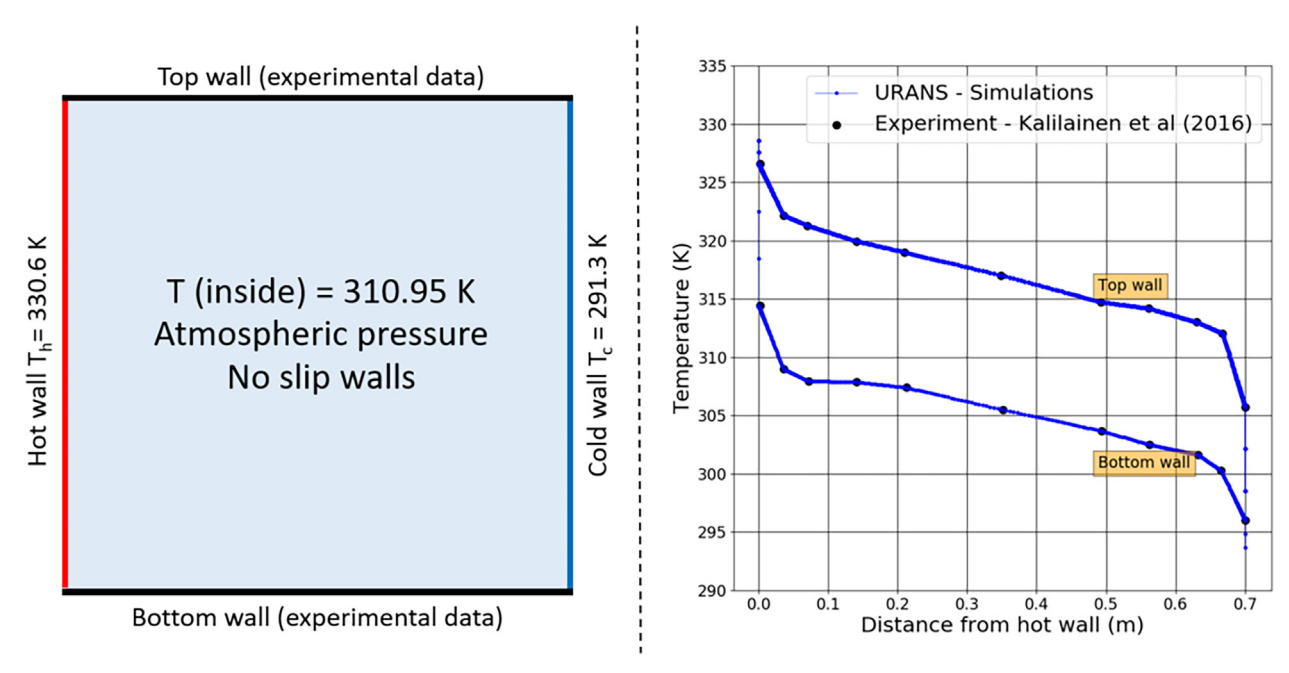


Fig. 4. DIANA experiment schematic and boundary conditions.

Table 2Mesh details for DIANA simulations

	Coarse mesh	Medium mesh	Fine mesh	BPGs [55]
Number of cells	125000	1000000	800000	
Average y+	1.98	1.12	0.58	
Maximum aspect ratio	99.5	98.72	97.52	<100
Maximum volume change	1.66	1.9	1.86	<8
Minimum face angle	90	90	90	>20
Maximum face angle	90	90	90	<160

circulation velocity (V_r) is defined as a function of thermal diffusivity of $air(\alpha)$, Rayleigh number (Ra) and side length of the cube (L) in Eq. 27.

$$\tau = \frac{L}{V_r} \tag{26}$$

$$V_r = \frac{\alpha\sqrt{Ra}}{L} \tag{27}$$

The flow field simulation are performed until 1200 nondimensional time units in total, while considering the final 600 non-dimensional time units for time averaging of results. The fluid flow mesh dependency is verified by computing Grid Convergence Index for global parameters such as average wall shear stress and integrated wall heat flux along hot and cold walls and local parameters like maximum velocity magnitude/temperature in the boundary layer. To conclude, the GCI index for medium mesh is approximately 0.1 % and the flow field computed from medium mesh is further utilized for computing particle transport. In the following results section, the velocity and temperature profiles from all the three meshes are plotted to emphasize that the medium and fine mesh yield almost identical results even though the computational efforts increased by 16 folds. However, the contour plots are only presented from the medium mesh. The medium mesh shown in Fig. 5 is the optimum mesh for the flow field and particle transport, and it has x_2^+ below one for the first cell in the boundary layer.

4. Results and discussion

In the current work, a systematic validation procedure is chosen to validate the Eulerian part (fluid flow) and the Lagrangian part (particle transport) of the CFD model separately by comparing with the experimental data. At first, the Eulerian part of the CFD model is validated by considering the velocity, turbulence intensity and temperature as the assessment parameters. In the following results and discussion, the profiles as well as the contours related to the fluid flow parameters belong to the central lateral plane (z = 0.35 m) of the cubical domain. Later, the Lagrangian part of the CFD model and implementation in the tailored CFD solver *containmentFOAM* is assessed by comparing the overall particle deposition and the distribution of remaining suspended particles in the domain.

4.1. Fluid Flow

The time-averaged mean velocity profiles at the mid height horizontal line (y = 0.35 m) from the CFD simulations is plotted together with the experimental data of Kalilainen et al. (2016) [15] (extracted from Dehbi et al. (2017) [18]) in Fig. 6.

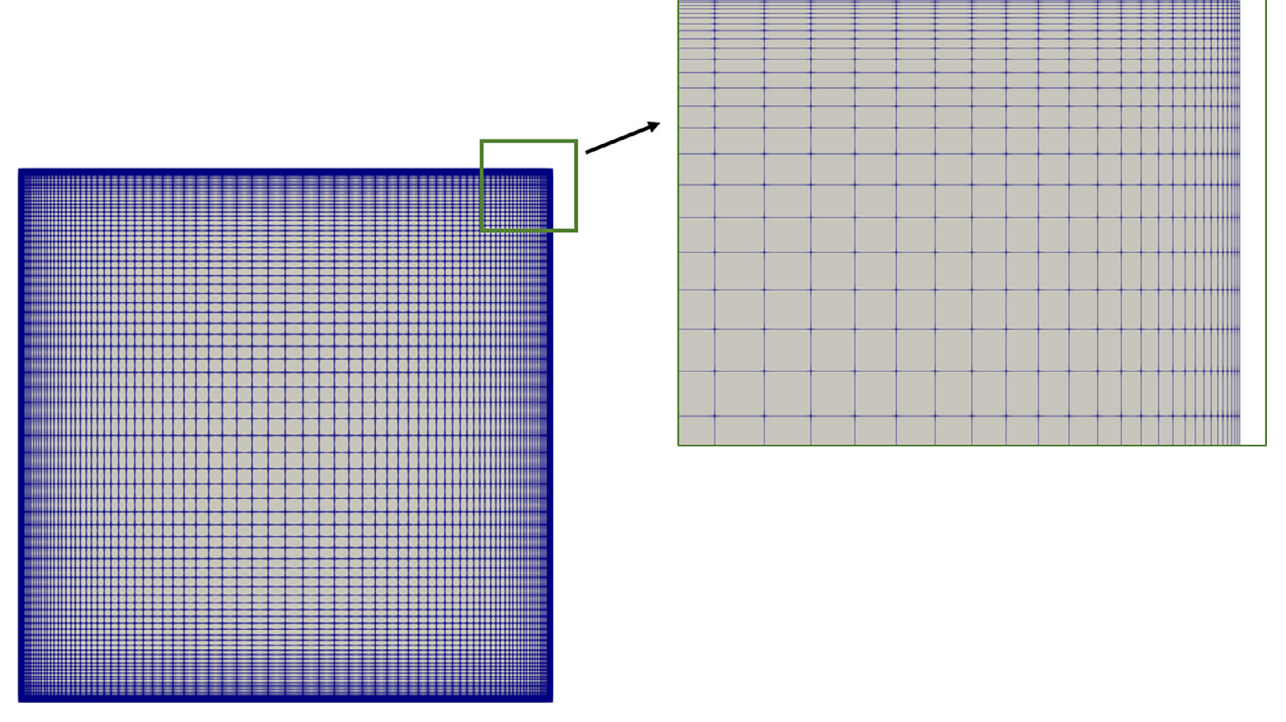


Fig. 5. Numerical mesh (medium) for DIANA simulations.

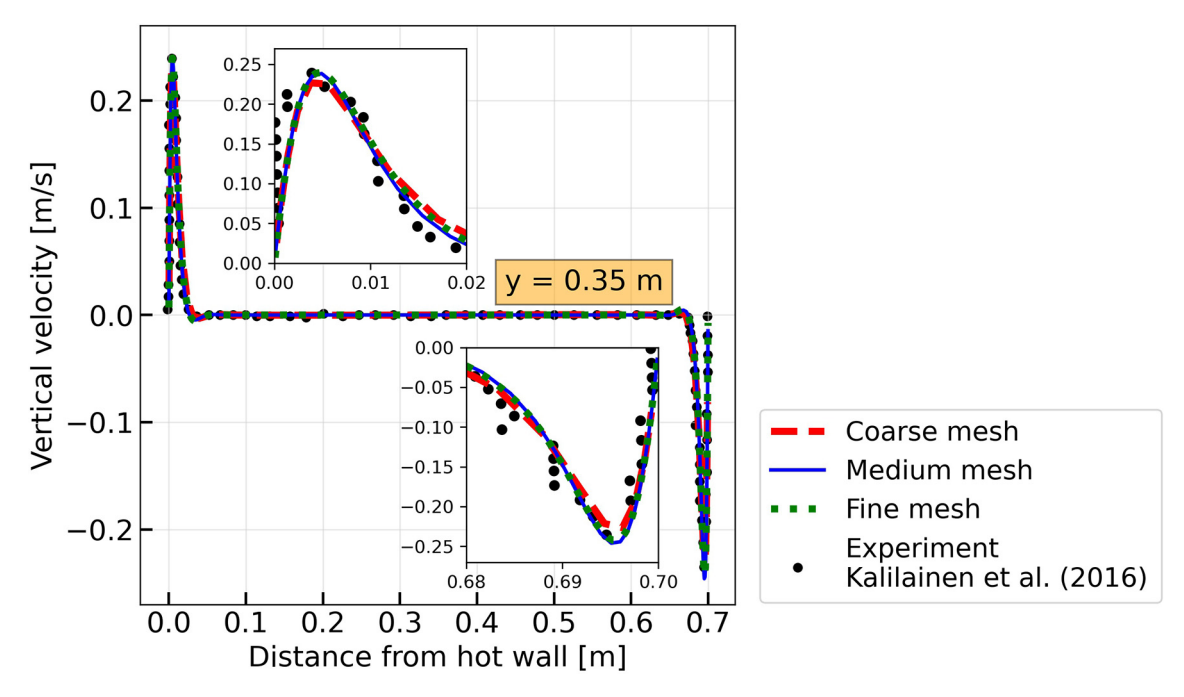


Fig. 6. Vertical velocity profile along the horizontal center line.

The mean velocity profiles from medium and fine meshes are close the experimental data, whereas the maximum velocity is slightly under-predicted in the coarse mesh simulation (shown in the subfigures of Fig. 6). The flow velocity magnitude reached a maximum of 0.25 m/s in the boundary layer along hot and cold walls and it mostly zero in the core region. In addition to the velocity profile along mid horizontal line, it is also important to have overall flow structure with reasonable accuracy in throughout the cavity for computing particle transport. The flow pattern is mostly two dimensional as the lateral front and back faces only have a minor influence. In this regard, the mean velocity contour from the medium mesh CFD simulation and experimental data are compared in Fig. 7.

In the experimental velocity magnitude contour from Kalilainen et al. (2016) [15] (left panel of Fig. 7), the scale is clipped to a maximum of 0.2 m/s. However, the comparison of the CFD simulation contour (right panel of Fig. 7) with the experiment shows that the flow structure is visually similar in both the cases, i.e, dominant

fluid flow mostly in the wall boundary layers and the core is almost still. It is worth to note that the secondary recirculation zones along the hot and cold walls are missing in the CFD simulation contour, which is an inherent deviation resulting from the RANS turbulence modeling approach. Recalling our objective to predict the particle deposition and distribution in a buoyancy driven flow accurately, the ability of current CFD model to predict the temperature variation within the flow domain is important. Prediction of temperature profiles plays a considerable in modeling the particles deposition pattern on walls. The thermophoretic force is comparable to drag force within the boundary layer of the flow along hot and cold walls, especially for submicron particles. As a consequence, temperature distribution also effects the airborne concentration of particles due to the change in temperature gradient in the boundary layer of flow.

The temperature distribution is measured in the DIANA cavity along five horizontal lines at different heights using K-type thermocouples and along the central vertical line. The CFD simulations

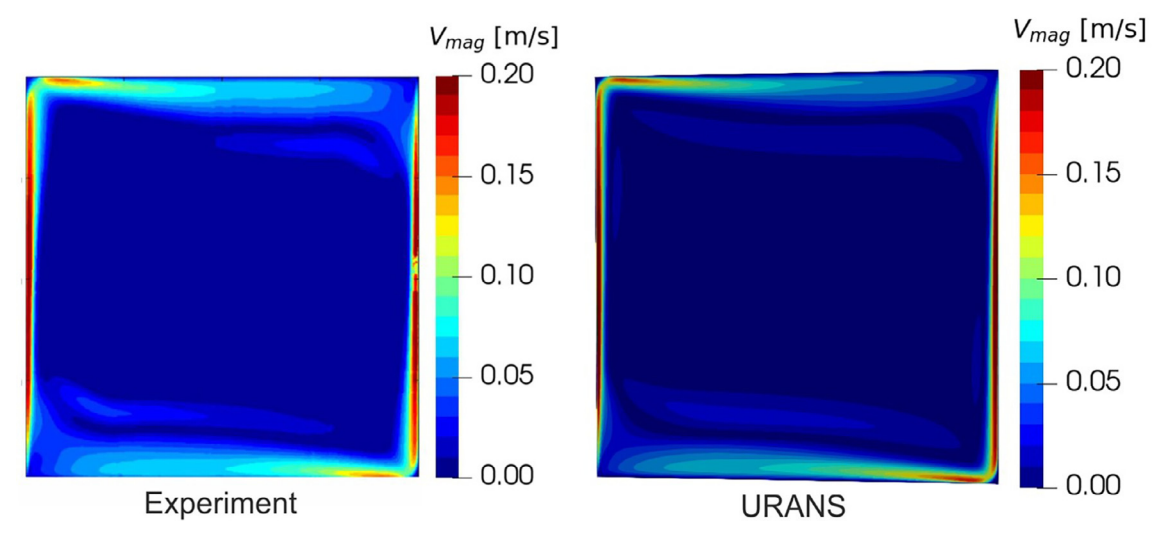


Fig. 7. Comparison of velocity magnitude contours between experiment and medium mesh simulation.

prediction of temperature distribution is plotted against the experimental data of Kalilainen et al. (2016) [15] in Figs. 8 and 9. On the left panel of Fig. 8, the temperature profiles along the horizontal lines at heights of 0.07 m, 0.21 m, 0.35 m, 0.49 m and 0.63 m are plotted in comparison with experimental data. In the bottom half of the domain, the temperature distribution is matching with the experimental data with less than 0.1 K difference. However, at the height of 0.49 m, there is a deviation of maximum 1.5 K in the core region and at the height of 0.63 m, there is a deviation of maximum 0.5 K. In order to visualize and assess the temperature deviation in the hot wall and cold wall boundary layers, the profiles are separately portrayed in the right panel of Fig. 8. For assessment of temperature variation in the vertical direction, the temperature profiles along the central vertical line (x = 0.35 m)is presented in comparison with the experimental data in Fig. 9. It should be noted that the mesh dependency in the temperature profiles is negligible (≤ 0.1 K). Based on the previous assessment of fluid velocity profile and the current temperature profiles, it can be concluded that medium mesh is sufficient to predict the temperature distribution (as well as the flow field) within 0.1 K error in the boundary layers.

4.2. Particle transport

The transient particle transport is simulated along with the flow. The particle tracking along is performed with Lagrangian time step (dt_{Lag}) in each fluid flow time step. It must be noted that the fluid flow time step is at least two order higher than the dt_{Lag} .

The particles are injected at 10,000 random locations distributed throughout the domain at non-dimensional time units τ = 600, when the flow is statistically steady. Particle tracking is performed up to 2000 s considering drag, gravity and thermophoretic forces along with the CRW model for turbulent dispersion. All the enclosure walls are treated as sticking surfaces for the particles. Two particle sizes 2.5 μ m and 1 μ m are simulated separately for validation against the experimental data from Kalilainen et al. (2016) [15] and Kim et al. (2018) [2]. The particle airborne concentration is computed as the fraction of suspended particles in flow to initial number of particles injected. The airborne concentration variations with time for 2.5 μ m and 1 μ m particles from CFD sim-

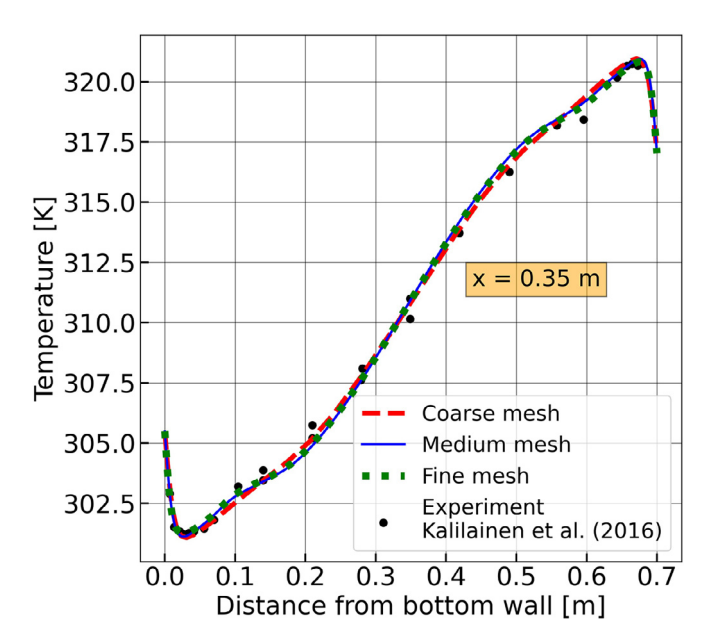


Fig. 9. Temperature variation along the central vertical line.

ulations are compared against the the experimental data and the simplistic stirred settling model in Figs. 10 and 11.

The stirred settling model is derived based on the assumption that the fluid in the enclosure is istropically agitated and the particles deposit only on the bottom surface due to the gravitational settling alone [56,15]. The decay constant (β_{TS}) of particles concentration obtained by the stirred settling model is defined as the ratio of terminal velocity of the particle to the side length (L) of the DIANA facility. The inverse of β_{TS} is the decay time constant (τ_{TS}) for the exponential decay of particles concentration.

$$\beta_{TS} = \frac{V_{TS}}{I} \tag{28}$$

$$\tau_{TS} = \frac{1}{\beta_{TS}} \tag{29}$$

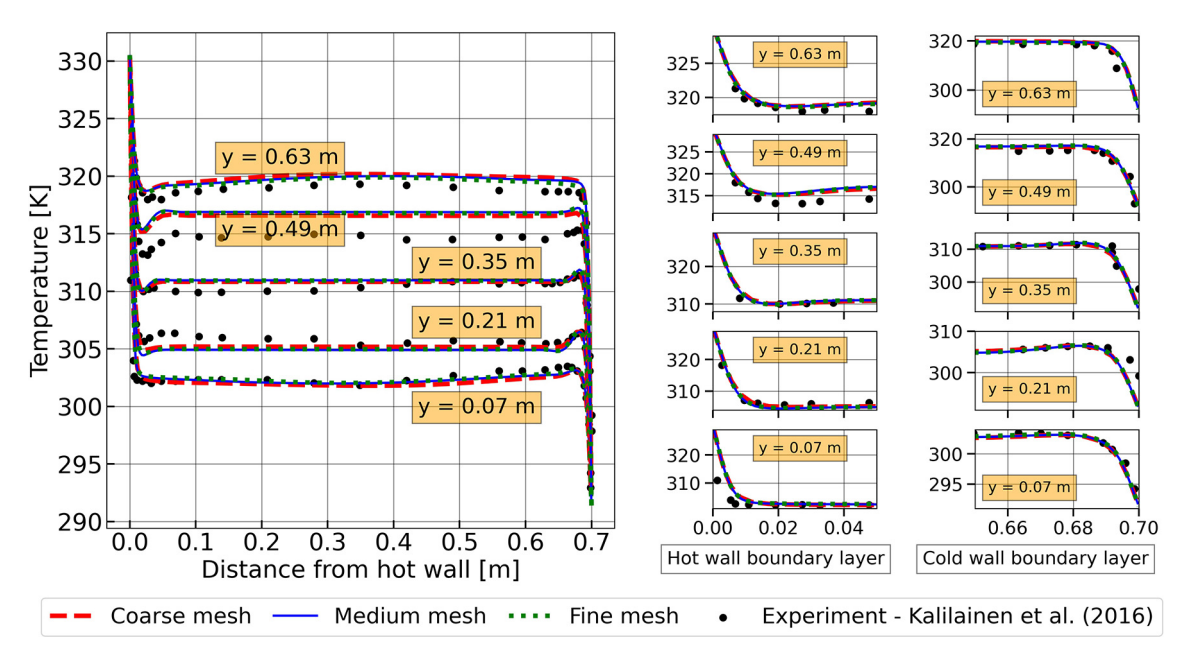


Fig. 8. Temperature variation along horizontal lines at different heights.

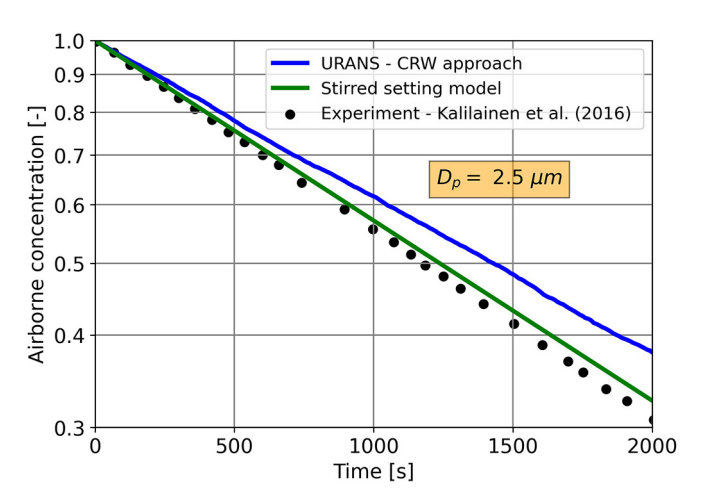


Fig. 10. 2.5 µm particles deposition in DIANA.

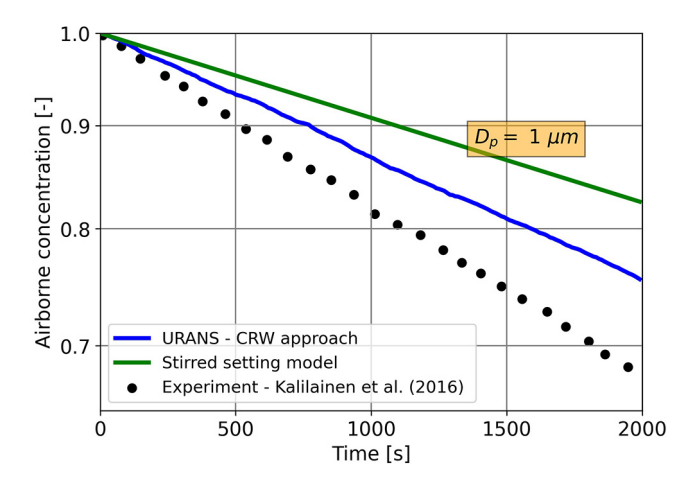


Fig. 11. 1 μm particles deposition in DIANA.

The particles airborne concentration at any time in the enclosure can be calculated using Eq. 2 and it is plotted for 2.5 μ m and 1 μ m particle sizes in Figs. 10 and 11 respectively.

As shown clearly in Fig. 10, The airborne concentration computed from stirred settling model is close to the experimental data in case of 2.5 µm particles, as the particle size is large enough to be not influenced by the turbulent diffusion. The CFD simulation gives a similar exponential decay of airborne concentration, but with a slightly slower rate of deposition for 2.5 µm particles. However, in the case of 1 µm particles (Fig. 11), the stirred settling model deviates significantly from the experimental data. This deviation is due to the considerable number of particles deposited on vertical walls (hot and cold walls) because of turbulent diffusion, and thermophoresis which are not considered in stirred settling model. On the other hand, the CFD simulation computes the airborne particle concentration closer to the experimental data than the stirred settling model. This shows the improvement in result due to the CRW model with RMS correlations from the DNS data. A simplified way of quantifying the whole deposition process is by calculating the time constant (τ) and it enables direct comparison with experimental data as well as simulations. In the following Tables 3, 4, the time constants obtained from the DIANA experiments using TEOM and Laser intensity methods by Kalilainen et al. (2016) [15] and by Kim et al. (2018) [2] using ELPI method are compared with present URANS-CRW result for 2.5 µm and 1 µm particles respectively. As a reference to modeling, the LES simulations

Table 3 Comparison of time constants and the resulted percentage of 2.5 μ m airborne particles after 2000 s from experiments and LES simulations to present URANS-CRW simulation

Method	Time constant for 2.5 μm particles (s)	Percentage of airborne particles
Experiment - TEOM [15]	1697 ± 86	30.8
Experiment - Laser intensity [15]	1796 ± 79	32.8
Experiment - ELPI [2]	1659 ± 89	29.9
Simulation - LES [18]	1616	29.0
Simulation - LES [2]	1618	29.0
Present simulation - URANS	2063	37.9
Stirred settling model	1784	32.6

Table 4 Comparison of time constants and the resulted percentage of 1 μ m airborne particles after 2000 s from experiments and LES simulations to present URANS-CRW simulation.

Method	Time constant for 1 μm particles (s)	Percentage of airborne particles
Experiment - TEOM [15]	5219 ± 188	68.2
Experiment - Laser intensity [15]	4965 ± 64	66.8
Experiment - ELPI [2]	6100 ± 411	72.1
Simulation - LES [18]	5297	68.5
Simulation - LES [2]	5291	68.5
Present simulation - URANS	7091	75.5
Stirred settling model	10210	82.5

predictions of time constants for DIANA by Dehbi et al. (2017) [18] and Kim et al. (2018) [2] and stirred settling model are also furnished in the same tables.

Based on the above data, the percentage of airborne particles of $2.5 \mu m$ size computed by the URANS-CRW approach is 5.1% - 8%more in comparison to the experiments after 2000 s. Similarly for 1 µm particles, the difference varies between 3.4% and 8.7%. In other words, the percentage error in computing the decay constant for 2.5 um particles is in the range of 14.9% –24.4%, and for 1 um particles is in the range of 16.2% - 42.8% by using URANS-CRW approach. Though the difference is significant, it is considerable improvement over the stirred settling model for 1 µm particles. It reiterates the fact that consideration of turbulent dispersion is important for submicron particles to assess their deposition on vertical walls. To understand further, the deposition on different walls are computed from the simulations and compared against the data from LES simulations of Dehbi et al. (2017 [18] and Kim et al. (2018) [2] in the following histograms (Figs. 12) and 13).

In case of 2.5 µm particles, the deposition is mostly on the bottom wall as predicted by both the present URANS-CRW approach and the LES model by Kim et al. (2018) [2]. The deposited fraction of particles on the cold wall is marginally lower in case of URANS-CRW approach in comparison to LES data. Though there was roughly 1% of particles deposited on the hot wall in LES simulation, the present URANS-CRW model couldn't reproduce such deposition on the hot wall. In the simulation of 1 µm particles, the deposition is almost equal on bottom wall and cold wall. This trend is predicted by both the current URANS-CRW model and the LES simulation by Dehbi et al. (2017) [18]. However, such deposition on bottom wall and cold wall predicted by URANS-CRW approach is slightly higher than the LES simulation by Dehbi et al. (2017) [18]. This is consequence of zero particle deposition on all other walls. The zero deposition on front and back walls can be associated with the two-dimensional nature of the flow field computed, while in experiments or LES, it is three dimensional.

In addition to the prediction of overall particles deposited, it is important to predict the particles distribution in the domain

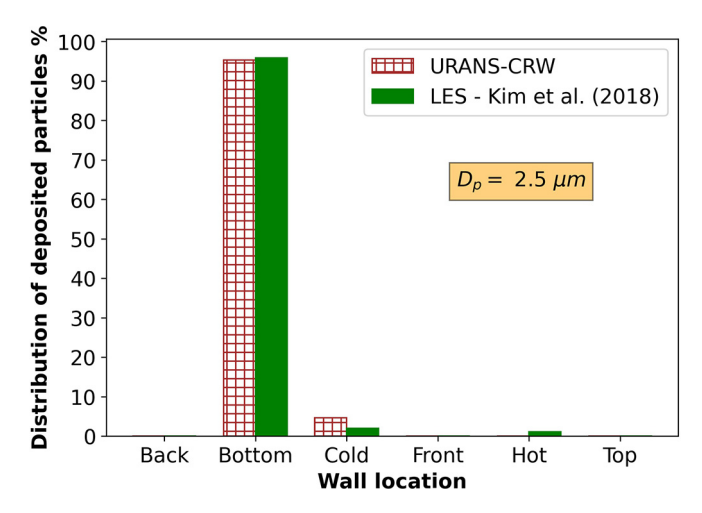


Fig. 12. wall-wise distribution of deposited 2.5 μm particles.

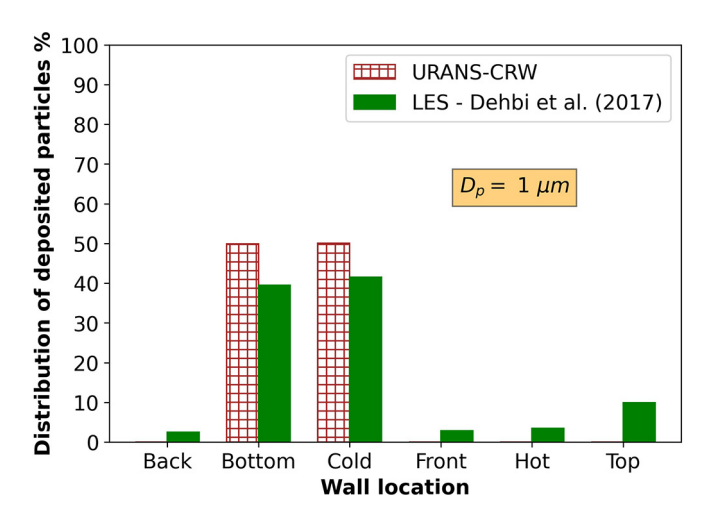


Fig. 13. wall-wise distribution of deposited 1 μm particles.

correctly. Liu (2010) [14] summarized large number of experiments and concluded that the airborne particles are uniformly distributed in enclosure flow at any time irrespective of the deposition rate. These findings are further confirmed by the LES simulations of DIANA experiments by Dehbi et al., (2017) [18] as well as the DIANA experiments [15]. In order to verify the particles distribution from current URANS simulations, the DIANA domain is divided into 64 cubicals (4 x 4 x 4) and relative particles concentration is computed. It is defined as the ratio of actual number of particles in that cubical to the mean number of particles per cubical (total number airborne particles divided by 64). In Fig. 14, a histogram of relative particle concentration in 64 cubicals at 500 s for 2.5 μ m is presented.

The mean and standard deviation are 1.0043 and 0.1129 respectively, which is close to a uniform distribution of suspended particles in the domain. Similarly for 1 μ m particles, a histogram of relative particle concentrations is plotted at 500 s in Fig. 15. The mean and standard deviation are for 1 μ m particles histogram are 1.0029 and 0.097 respectively, which represent very close uniform distribution of particles in all the cubicals. LES simulations of the DIANA experiment for 1 μ m particles revealed that the standard deviation of a similar histogram at 2000 s is 0.05 [18]. The difference could be attributed to the superiority of LES method in capturing the turbulence levels and re-circulation zones over the URANS approach and also to the smaller particle sample used for

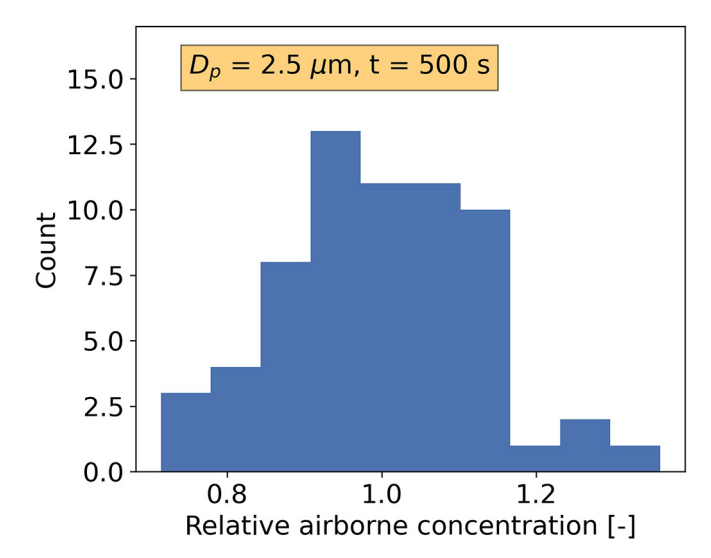


Fig. 14. 2.5 µm particles distribution in DIANA.

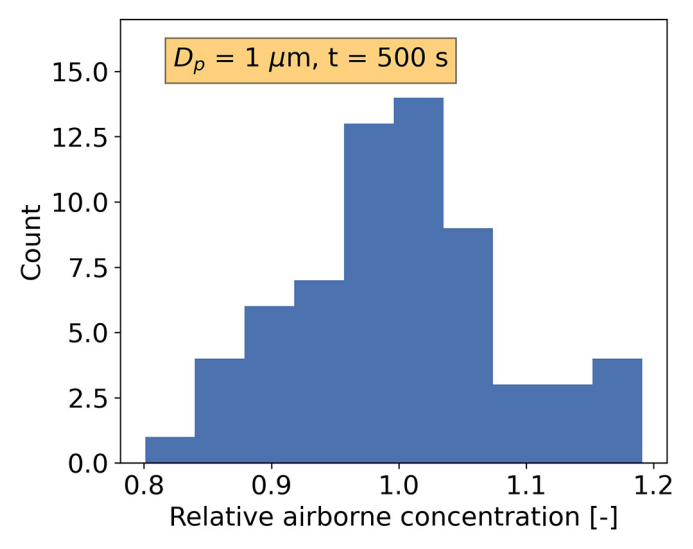


Fig. 15. 1 μm particles distribution in DIANA.

URANS (10000) versus LES (100000). Nonetheless, the results demonstrated the capability of the CRW model to assess particle transport and deposition in buoyancy driven flows. Due to its computational efficiency, URANS can be employed in future to technical scale applications.

5. Summary and conclusions

In the present work, an Eulerian–Lagrangian approach is employed to compute particle transport and deposition in a buoyancy driven flow. For the Eulerian part, the baseline CFD model based on the k- ω SST model, which is well validated for the containment flows, is applied. In the Lagrangian particle tracking, drag, gravity, thermophoresis and turbulent dispersion are considered. For the turbulent dispersion modeling, the well known continuous random walk model based on normalized Langevin equations is utilized with appropriate RMS velocity correlations derived from the DNS data of Sebilleau et al. (2018) [50]. With this, the application of (U) RANS - CRW combined approach is extended to particle transport in natural convection turbulent flow. The models are

implemented in a tailored CFD solver for containment flows *containmentFOAM* to extend its applicability to particle-laden flows.

This approach is validated against the DIANA experimental data of Kalilainen et al. (2016) [15] for 1 μm and 2.5 μm particle sizes, and the results are satisfactory in predicting particle deposition on enclosure surfaces and overall distribution in the domain. Further more, the approach is numerically more efficient than LES, which is of significance for future technical scale applications. Nevertheless, it must be noted that while a further utilization of this modeling approach for tracking aerosols in large scale enclosures is feasible, one needs to verify the scalability of current RMS velocity correlations to different geometries depending on Rayleigh number.

Declaration of Competing Interest

The authors declare that they have no known competing financial interests or personal relationships that could have appeared to influence the work reported in this paper.

Acknowledgements

The extensive experiments in the DIANA facility were conducted by the Laboratory of the Scientific Computing and Modeling at Paul Scherrer Institut (Switzerland). The authors gratefully thank Dr. J. Kalilainen for the discussion on experiments. The authors express their profound appreciation to Ms. Astrid Kuhr for her technical assistance in handling the super computing facility at Forschungszentrum Jülich. The authors acknowledge the HITEC Graduate School at Forschungszentrum Jülich for providing the funding partially for the doctoral position.

References

- [1] A. Islas, A. Rodríguez-Fernández, C. Betegón, E. Martínez-Pañeda, A. Pandal, Cfd simulations of turbulent dust dispersion in the 20 l vessel using openfoam, Powder Technol. 397 (2022) 117033.
- [2] H. Kim, A. Dehbi, J. Kalilainen, Measurements and les computations of a turbulent particle-laden flow inside a cubical differentially heated cavity, Atmos. Environ. 186 (2018) 216–228.
- [3] V. Vuorinen, M. Aarnio, M. Alava, V. Alopaeus, N. Atanasova, M. Auvinen, N. Balasubramanian, H. Bordbar, P. Erästö, R. Grande, N. Hayward, A. Hellsten, S. Hostikka, J. Hokkanen, O. Kaario, A. Karvinen, I. Kivistö, M. Korhonen, R. Kosonen, J. Kuusela, S. Lestinen, E. Laurila, H.J. Nieminen, P. Peltonen, J. Pokki, A. Puisto, P. Råback, H. Salmenjoki, T. Sironen, M. Österberg, Modelling aerosol transport and virus exposure with numerical simulations in relation to sarscov-2 transmission by inhalation indoors, Saf. Sci. 130 (2020) 104866.
- [4] M. Abuhegazy, K. Talaat, O. Anderoglu, S.V. Poroseva, Numerical investigation of aerosol transport in a classroom with relevance to covid-19, Phys. Fluids 32 (2020) 103311.
- [5] M. Horn, H.-J. Schmid, A comprehensive approach in modeling lagrangian particle deposition in turbulent boundary layers, Powder Technol. 186 (2008) 189–198.
- [6] M. Rybalko, E. Loth, D. Lankford, A lagrangian particle random walk model for hybrid rans/les turbulent flows, Powder Technol. 221 (2012) 105–113, Selected papers from 2010 AIChE Annual Meeting.
- [7] M. Aksouh, A. Dehbi, Large eddy simulations of particulate flows inside a square differentially heated cavity at rayleigh numbers up to 1011, Powder Technol. 336 (2018) 318–331.
- [8] M. Ihalainen, T. Lind, J. Ruusunen, P. Tiitta, A. Lähde, T. Torvela, J. Jokiniemi, Experimental study on bounce of submicron agglomerates upon inertial impaction, Powder Technol. 268 (2014) 203–209.
- [9] Q. Ma, Y. Zhou, H. Gu, Z. Sun, H. Liang, H. Zhou, Experimental research on aerosol scrubbing characteristics in the submerged jet under high pool pressure, Powder Technol. 415 (2023) 118170.
- [10] S. Mao, T. Zhou, Y. Liao, J. Tang, X. Liu, Thermal-hydraulic and particle deposition analysis of supercritical co2 in different tubes, Powder Technol. 413 (2023) 118076.
- [11] P. Fevrier, O. Simonin, K.D. Squires, Partitioning of particle velocities in gassolid turbulent flows into a continuous field and a spatially uncorrelated random distribution: theoretical formalism and numerical study, J. Fluid Mech. 533 (2005) 1–46.

- [12] P.S. Goswami, V. Kumaran, Particle dynamics in the channel flow of a turbulent particle–gas suspension at high stokes number. part 1. dns and fluctuating force model, J. Fluid Mech. 687 (2011) 1–40.
- [13] J.D. Kulick, J.R. Fessler, J.K. Eaton, Particle response and turbulence modification in fully developed channel flow, J. Fluid Mech. 277 (1994) 109– 134
- [14] D.-L. Liu, Chapter 1-particle deposition onto enclosure surfaces (2010) 1–56.
- [15] J. Kalilainen, P. Rantanen, T. Lind, A. Auvinen, A. Dehbi, Experimental investigation of a turbulent particle-laden flow inside a cubical differentially heated cavity, J. Aerosol Sci. 100 (2016) 73–87.
- [16] B.T. Chen, H.C. Yeh, Y.S. Cheng, Evaluation of an environmental reaction chamber, Aerosol Sci. Technol. 17 (1992) 9–24.
- [17] T.L. Thatcher, W.A. Fairchild, W.W. Nazaroff, Particle deposition from natural convection enclosure flow onto smooth surfaces, Aerosol Sci. Technol. 25 (1996) 359–374.
- [18] A. Dehbi, J. Kalilainen, T. Lind, A. Auvinen, A large eddy simulation of turbulent particle-laden flow inside a cubical differentially heated cavity, J. Aerosol Sci. 103 (2017) 67–82.
- [19] J. Pallares, F. Grau, Particle dispersion in a turbulent natural convection channel flow, J. Aerosol Sci. 43 (2012) 45–56.
- [20] R. Puragliesi, A. Dehbi, E. Leriche, A. Soldati, M. Deville, Dns of buoyancy-driven flows and lagrangian particle tracking in a square cavity at high rayleigh numbers, Int. J. Heat Fluid Flow 32 (2011) 915–931.
- [21] M.A. Sayed, A. Dehbi, M. Hadžiabic, B. Niceno, K. Mikityuk, Cfd simulation of particle-laden flow in a 3d differentially heated cavity using coarse large eddy simulation, Flow, Turbul. Combust. 109 (2022) 961–990.
- [22] A. Dehbi, Turbulent particle dispersion in arbitrary wall-bounded geometries: A coupled cfd-langevin-equation based approach, Int. J. Multiph. Flow 34 (2008) 819–828.
- [23] A. Dehbi, A stochastic langevin model of turbulent particle dispersion in the presence of thermophoresis, Int. J. Multiph. Flow 35 (2009) 219–226.
- [24] A. Dehbi, Validation against dns statistics of the normalized langevin model for particle transport in turbulent channel flows, Powder Technol. 200 (2010) 60– 68
- [25] A. Dehbi, F. de Crécy, Validation of the langevin particle dispersion model against experiments on turbulent mixing in a t-junction, Powder Technol. 206 (2011) 312–321.
- [26] S. Jayaraju, P. Sathiah, F. Roelofs, A. Dehbi, Rans modeling for particle transport and deposition in turbulent duct flows: Near wall model uncertainties, Nucl. Eng. Des. 289 (2015) 60–72.
- [27] R. Mukin, A. Dehbi, Particle deposition modeling in the secondary side of a steam generator bundle model, Nucl. Eng. Des. 299 (2016) 112–123, CFD4NRS-
- [28] A.A. Mofakham, G. Ahmadi, On random walk models for simulation of particle-laden turbulent flows, Int. J. Multiph. Flow 122 (2020) 103157.
- [29] C. Lo, J. Bons, Y. Yao, J. Capecelatro, Assessment of stochastic models for predicting particle transport and deposition in turbulent pipe flows, J. Aerosol Sci. 162 (2022) 105954.
- [30] S. Kelm, M. Kampili, X. Liu, A. George, D. Schumacher, C. Druska, S. Struth, A. Kuhr, L. Ramacher, H.-J. Allelein, K.A. Prakash, G.V. Kumar, L.M.F. Cammiade, R. Ji, The tailored cfd package 'containmentfoam' for analysis of containment atmosphere mixing, h2/co mitigation and aerosol transport, Fluids 6 (2021).
- [31] G. Vijaya Kumar, M. Kampili, S. Kelm, K. Arul Prakash, H.-J. Allelein, Cfd modelling of buoyancy driven flows in enclosures with relevance to nuclear reactor safety, Nucl. Eng. Des. 365 (2020) 110682.
- [32] M. Kampili, G. Vijaya Kumar, S. Kelm, K. Arul Prakash, H.-J. Allelein, Cfd simulations of stratified layer erosion in minipanda facility using the tailored cfd solver containmentfoam, Int. J. Heat Mass Transf. 178 (2021) 121568.
- [33] X. Liu, S. Kelm, M. Kampili, G.V. Kumar, H.-J. Allelein, Monte carlo method with snbck nongray gas model for thermal radiation in containment flows, Nucl. Eng. Des. 390 (2022) 111689.
- [34] K. Yassin, S. Kelm, M. Kampili, E.-A. Reinecke, Validation and verification of containmentfoam cfd simulations in hydrogen safety, Energies 16 (2023).
- [35] C. Fiorina, I. Clifford, S. Kelm, S. Lorenzi, On the development of multi-physics tools for nuclear reactor analysis based on openfoam®: state of the art, lessons learned and perspectives, Nucl. Eng. Des. 111604 (2021).
- [36] P. Le Queré, M. Behnia, From onset of unsteadiness to chaos in a differentially heated square cavity, J. Fluid Mech. 359 (1998) 81–107.
- [37] G. Bagheri, M. Salmanzadeh, V. Golkarfard, G. Ahmadi, Simulation of solid particles behavior in a heated cavity at high rayleigh numbers, Aerosol Sci. Technol. 46 (2012) 1382–1391.
- [38] L. Schiller, A. Naumann, uber die grundlegenden berechnungen bei der schwerkraftaufbereitung, Verein Deutscher Ingenieure (1933).
- [39] F. Greifzu, C. Kratzsch, T. Forgber, F. Lindner, R. Schwarze, Assessment of particle-tracking models for dispersed particle-laden flows implemented in openfoam and ansys fluent, Eng. Appl. Comput. Fluid Mech. 10 (2016) 30–43.
 [40] L. Talbot, R.K. Cheng, R.W. Schefer, D.R. Willis, Thermophoresis of particles in a
- [40] L. Talbot, R.K. Cheng, R.W. Schefer, D.R. Willis, Thermophoresis of particles in a heated boundary layer, J. Fluid Mech. 101 (1980) 737–758.
- [41] A. Obukhov, Description of turbulence in terms of lagrangian variables, volume 6 of Advances in Geophysics, Elsevier, 1959, pp. 113–116.
- [42] R. Thompson, Numeric calculation of turbulent diffusion, Quart. J. Roy. Meteorol. Soc. 97 (1971) 93–98.
- [43] J.D. Wilson, G.W. Thurtell, G.E. Kidd, Numerical simulation of particle trajectories in inhomogeneous turbulence, i: Systems with constant turbulent velocity scale, Boundary-Layer Meteorol 21 (1981) 295–313.

- [44] B.J. Legg, M.R. Raupach, Markov-chain simulation of particle dispersion in inhomogeneous flows: The mean drift velocity induced by a gradient in eulerian velocity variance, Boundary-Layer Meteorol 24 (1982) 3–13.
- [45] D.J. Thomson, Random walk modelling of diffusion in inhomogeneous turbulence, Quart. J. Royal Meteorol. Soc. 110 (1984) 1107–1120.
- [46] I. Iliopoulos, Y. Mito, T.J. Hanratty, A stochastic model for solid particle dispersion in a nonhomogeneous turbulent field, Int. J. Multiph. Flow 29 (2003) 375–394.
- [47] Y. Mito, T. Hanratty, Use of a modified langevin equation to describe turbulent dispersion of fluid particles in a channel flow, Flow, Turbul. Combust. 68 (2002) 1–26.
- [48] D.J. Thomson, Criteria for the selection of stochastic models of particle trajectories in turbulent flows, J. Fluid Mech. 180 (1987) 529–556.
- [49] Y. Mito, T.J. Hanratty, A stochastic description of wall sources in a turbulent field: part 2. calculation for a simplified model of horizontal annular flows, Int. J. Multiph. Flow 30 (2004) 803–825, A Collection of Papers in Honor of Professor G. Yadigaroglu on the Occasion of his 65th Birthday.

- [50] F. Sebilleau, R. Issa, S. Lardeau, S.P. Walker, Direct numerical simulation of an air-filled differentially heated square cavity with rayleigh numbers up to 1011, Int. J. Heat Mass Transf. 123 (2018) 297–319.
- [51] T. Bocksell, E. Loth, Stochastic modeling of particle diffusion in a turbulent boundary layer, Int. J. Multiph. Flow 32 (2006) 1234–1253.
- [52] G. Kallio, M. Reeks, A numerical simulation of particle deposition in turbulent boundary layers, Int. J. Multiph. Flow 15 (1989) 433–446.
- [53] M. Kampili, S. Kelm, A. Dehbi, H.-J. Allelein, Development of a continuous random walk model based on normalized langevin equation in openfoam for turbulent dispersion of particles and validation against dns statistics, 7th OpenFOAM conference (ESI), Berlin, Germany, October 15 - 17.
- [54] A. Dehbi, S. Kelm, J. Kalilainen, H. Mueller, The influence of thermal radiation on the free convection inside enclosures, Nucl. Eng. Des. 341 (2019) 176–185.
- [55] J. Mahaffy, et al, Best practice guidelines for the use of cfd in nuclear reactor safety applications - revision, NEA/CSNI/R(2014) 11.
- [56] W.C. Hinds, Aerosol technology: Properties, behavior, and measurement of airborne particles, Second edition (1999).